VoroNoodles: Topological Interlocking with Helical Layered 2-Honeycombs

Matthew Ebert, Ergun Akleman, Vinayak Krishnamurthy, Roman Kulagin, and Yuri Estrin*

An approach for modeling topologically interlocked building blocks that can be assembled in a water-tight manner (space filling) to design a variety of spatial structures is introduced. This approach takes inspiration from recent methods utilizing Voronoi tessellation of spatial domains using symmetrically arranged Voronoi sites. Attention is focused on building blocks that result from helical stacking of planar 2-honeycombs (i.e., tessellations of the plane with a single prototile) generated through a combination of wallpaper symmetries and Voronoi tessellation. This unique combination gives rise to structures that are both space-filling (due to Voronoi tessellation) and interlocking (due to helical trajectories). Algorithms are developed to generate two different varieties of helical building blocks, namely, corrugated and smooth. These varieties result naturally from the method of discretization and shape generation and lead to distinct interlocking behavior. In order to study these varieties, finite-element analyses (FEA) are conducted on different tiles parametrized by 1) the polygonal unit cell determined by the wallpaper symmetry and 2) the parameters of the helical line generating the Voronoi tessellation. Analyses reveal that the new design of the geometry of the building blocks enables strong variation of the engagement force between the blocks.

1. Introduction

1.1. Context and Motivation

The concept of topological interlocking was introduced in an article by Dyskin et al.[1] The area of topological interlocking design has matured over the 20 years since that publication. A brief overview of these developments was presented recently.[2] It was posited that a huge repository of engineering structures could be built up by designing segmented structures consisting of interlocked elements. Here we present one such structure, based on tessellating a plane and proliferating the prototype tiles ("prototiles") in the third dimension according to helical movement and stacking of 2D space-filling tessellations, generally defined as 2-honeycombs in the geometry of tessellations.

Tiling and tessellations are central to many applications such as the design of architectural forms, functional/architectured materials (materials whose behavior is dictated by the geometric arrangement of material rather than its microscale constitutive properties).[3,4] This article focuses on space-filling topologically interlocking blocks, special class shapes that tessellate volumetric domains. Topologically interlocking assemblies are composed of blocks that stay in place purely due to the kinematic constraints imposed by their neighboring blocks under a peripheral force. While several prior studies have demonstrated topologically interlocked assemblies using polyhedral blocks (**Figure 1**), we observe that recent works have introduced topological interlocking with space-filling blocks.[5,6] The motivation for our work stems from the observation that these

M. Ebert, V. Krishnamurthy
J. Mike Walker '66 Department of Mechanical Engineering
Texas A&M University
100 Mechanical Engineering Office Building, College Station, TX 77843, USA

E. Akleman
Visual Computing and Computational Media
Texas A&M University
798 Ross Street, College Station, TX 77843, USA

E. Akleman, V. Krishnamurthy
Department of Computer Science (By Affiliation)
Texas A&M University
435 Nagle Street, College Station, TX 77843, USA

R. Kulagin
Institute of Nanotechnology
Karlsruhe Institute of Technology
Hermann-von-Helmholtz-Platz 1, 76344 Eggenstein-Leopoldshafen, Germany

Y. Estrin
Department of Materials Science and Engineering
Monash University
Clayton, VIC 3800, Australia
E-mail: yuri.estrin@monash.edu

Y. Estrin
Department of Mechanical Engineering
The University of Western Australia
Crawley 6009, Australia

recent works either do not guarantee complete topological interlocking (i.e., only a subset of the shapes interlock in more than one direction/dimension)[5] or utilize special spatial symmetries (e.g., wallpaper[5] or weaves[6]) to generate such blocks. In this article, the goal is to enable the generation of space-filling shapes through methods that are 1) guaranteed to produce strong topological interlocking through corrugation and 2) leverage simple geometric principles that are not selective regarding the type of one or the other spatial symmetry (**Figure 2**).

Toward our goal, we introduce a novel approach for generating space-filling corrugated blocks that resemble noodle-like structures, resulting in strong topological interlocking assemblies. Our approach is based on decomposing a given volume using helical ruled surfaces as Voronoi sites that populate volume using Bravais lattices. The shapes are still obtained by layer-by-layer Voronoi decomposition (see Figure 13), which is also critical for obtaining strong corrugation. Layer-by-layer Voronoi decomposition guarantees obtaining genus-0 surfaces, and the resulting blocks can always be assembled. An important property of this approach is that it provides access to a large design space for producing topologically interlocking tessellations.

Using this approach, we introduce two unique varieties, namely constant cross-sectional noodles (shapes that have the same cross sections akin to a swept volume, **Figure 3**) and variable cross-sectional noodles (shapes that have varying cross sections akin to lofted volumes, **Figure 4**). This flexibility in design space is quite helpful to systematically search for new tessellated forms.

1.2. Background

Our work lies at the intersection of many of these rich domains of interlocking structures, bioinspired structures, as well as space-filling structures. Interlocking is a common template in natural materials and structures such as bone structures, teeth, and shelled creatures (e.g., moluscs).[7] One of the main advantages of this template is that interlocked mechanical elements enable multiple desired mechanical behaviors pertaining to stiffness and toughness, leading to exciting avenues in bioinspired structural materials[8] and bone tissue engineering.[9,10] Layered ceramics have also been used to create structures with interesting mechanical responses compared to a monolithic counterpart.[11] In a similar vein, laminations have been used
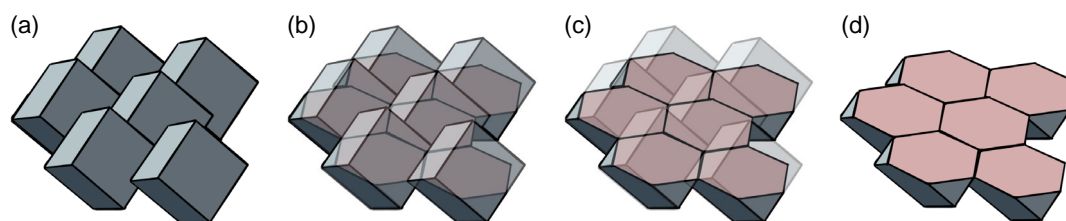

Figure 1. A topological interlocking assembly of cubes.[2] Similar assemblies for other regular polyhedra (the Platonic bodies) were discovered.[2] In this assembly, there exists a plane that can provide us a cell-transitive 2-honeycomb, which can be used to apply a peripheral force. a) Assembly, b) Transparent view 1; c) Transparent view 2; d) Cell-transitive 2-honeycombs. Reproduced under terms of the CC BY-NC-ND 4.0, Copyright 2021, published by Yuri Estrin, Vinayak Krishnamurthy, and Ergun Akleman.
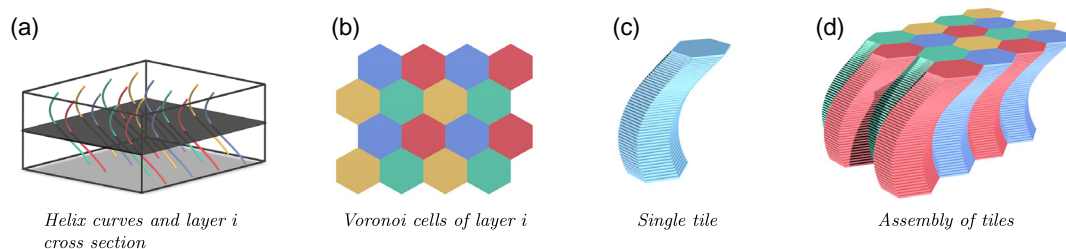

Helix curves and layer i cross section   *Voronoi cells of layer i*   *Single tile*   *Assembly of tiles*

Figure 2. a) The generation of VoroNoodles is shown where several helices are placed inside an architectured slab, and b) the Voronoi tessellation is computed at each layer i. c) A tile is created by extruding each layer i, and d) multiple tiles form an assembly.
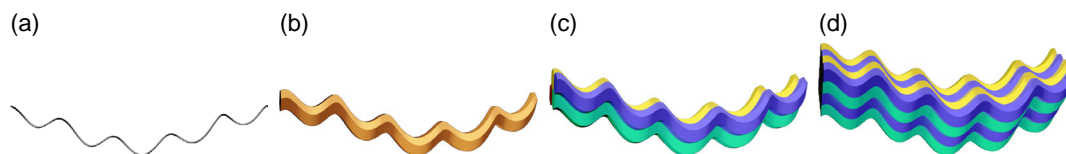

Figure 3. An example of constant cross-section VoroNoodles as an extruded 2-honeycomb. Since the 2-honeycomb is exactly the same in each layer, each congruent block is exactly the same in each layer. Since it is generated using a single curve, the resulting congruent blocks in each layer are convex polygons. In this particular case. they are all regular hexagons. Each layer is translated using this parametric equation: $x = 2\cos(2\pi t) + \cos(2\pi 5t)$, $y = 2\sin(2\pi t) + \sin(2\pi 5t)$, and $z = 4t$. We used $|v_0| \ll 1$ and $|v_1| \ll 1$ to obtain a long and skinny spaghetti look. a) Single curve; b) A single constant cross section noodle; c) 2×2 assembly of constant cross section noodle; d) 4×4 assemble of constant cross section noodle.
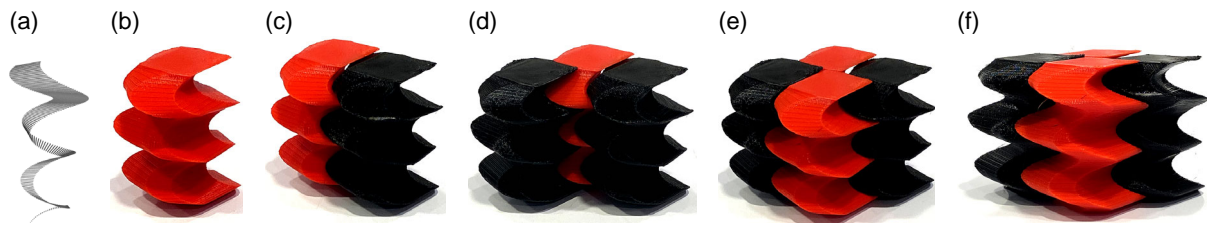
Figure 4. An example of congruent VoroNoodles that provide strong topological interlocking. Each layer is translated into a parametric equation in the form of $x = \cos(3z)$ and $y = \sin(3z)$ to produce a helix. To obtain the helical ruled surface shown in (a), we rotated and scaled a 2D vector along this helix. Translated versions of these ruled surfaces are used as Voronoi sites to obtain VoroNoodles. a) Ruled surface; b) A printed VoroNoodle; c) Two printed VoroNoodles d) Assembly of three printed VoroNoodles. e) 2×2 assembly of VoroNoodles; f) 2×2 assembly of printed VoroNoodles. Reproduced under terms of the CC BY-NC-ND 4.0, Copyright 2022, published by Cassie Mullins, Matthew Ebert, Ergun Akleman, and Vinayak Krishnamurthy.[63]

to create multilayered tiles of layered ceramics.[12] A related class of materials are random fibrous structures having high fracture toughness,[13] similar to that of topologically interlocked structures. Due to this, there is interest in such materials for applications in various areas, including acoustics[14] and heat transfer.[15] Another direction where we find significant interest in interlocked geometries is in the domain of textile fabrics and composite structures based on such fabrics.[16,17] Woven structures have been used to create architectured materials through defining their weaving symmetry[18] as well as the use of interlocking tiles.[6,19] These woven structures have a deep history of use for many fabric patterns and clothing items. The last piece of our puzzle comes from recent work on space-filling granular crystals which have the potential to be used as modular building blocks to enable intriguing mechanical responses.[20] Taking inspiration from these closely linked structural design concepts of interlocking, our further goal in this work is to assimilate corrugation as a new aspect within the design of space-filling topologically interlocked structures.

1.3. Basis and Rationale

Our general idea is based on using helical shapes as Voronoi cells. To picture mentally how we get corrugated block regions, imagine that N helices are screwed into a thick architectured shell or slab. We partition this shell into N block regions where region i consists of all points closest to helix number i. This operation naturally creates desired corrugated boundaries between the block regions. It should be clear that shapes and placements of helices play important roles in obtaining interesting corrugated blocks.

The first requirement is that no two helices (or "screws") intersect with each other. This is not physically possible, but our virtual screws can potentially intersect each other if we place them randomly. To obtain a meaningful decomposition of the space, we also need screws to be placed as uniformly as possible inside of the shell. This means no two screws have to be too close to each other and there should not be any large region left without a screw. Boris Delaunay introduced the concept of "Delone Set" to formally describe such as-uniform-as-possible placements[21–23] (note the two different spellings of the name of this great mathematician in literature).

Delaunay's concept involves two principles: 1) uniformly discrete and 2) relatively dense, to define as-uniform-as-possible placements of points. Let S denote a set of points in n-dimensional Euclidean space, $\Re^n$. S is called a Delone set if it is both uniformly discrete and relatively dense.[24] Let $r_1 > r_0$ denote two positive numbers: then 1) the point set S is uniformly discrete if each sphere of radius r_0 contains at most one point in S; 2) the point set S is relatively dense if every sphere of radius r_1 contains at least one point of S.[25] If we use the points in $S \in \Re^3$ as Voronoi sites, we can obtain a nice tessellation of space. This partition is "nice" in the sense that the resulting Voronoi cells are similarly sized convex polyhedra.

Even though the notions uniformly discrete and relatively dense are defined and can be intuitively understood for points only, they are still useful if the sizes of higher-dimensional Voronoi sites are much smaller than r_0, where we can define the size of the object as the radius of a bounding sphere. Our problem, however, requires an alternative approach. If the screws are far away from each other, they will act like points so that boundaries between Voronoi regions will not have many corrugations. In order to produce corrugated boundaries, we need to place screws as-close-as-possible. In this case, the sizes and shapes of the screws play an important role in obtaining uniformly discrete and relatively dense distributions.

To solve this problem, we make a set of simplifications. We represent shells/slabs as a tensor-product B-spline volume that is obtained by bijective mapping. The screws are obtained by the same bijective mapping of curves and ruled surfaces that are defined in parametric domain $(x, y, z) \in [0, 1]^3$. They are defined by a trigonometric function to control frequency of corrugation intuitively. The intersection of a screw with any z constant plane is guaranteed to be a point or a line. With points and lines, it is easy to obtain uniformly discrete and relatively dense distribution in each plane. This further allows one to pack long curves or ruled surfaces as close as possible to each other without intersection.

For placement and arrangement of the Voronoi sites, we employ a strategy developed by Auguste Bravais[26] that enables populating the system using only translations. Using Bravais lattices, symmetric Delone sets in the parametric domain are obtained.[22] Because of symmetry, the Voronoi decomposition of the parametric domain results in a Voronoi tessellation that consists of congruent blocks.

2300831 (3 of 12)

1.4. Challenges and Approach

Even though previous works have employed similar approaches to obtain topologically interlocking tiles such as Delaunay lofts and generalized Abeille tiles (GATs),[5,6] they do not provide corrugated boundaries. Rather, topological interlocking is provided by the global structure. Utilizing helical ruled surfaces as Voronoi sites does lead to intuitive and generalizable design mechanisms to obtain desired corrugated boundaries. For instance, an intuitive way of defining such a ruled surface is rotating and scaling a line while translating its center. To demonstrate this intuitive approach, we choose a concrete class of helical trajectories wherein we map the motion of each Voronoi site based on the transformation matrices induced by the helix. Our results show that the ensuing congruent shapes coming from helical trajectories have great potential for topological interlocking assemblies by providing corrugated boundaries.

2. Prior Work

2.1. Topological Interlocking in Mechanics

Topological interlocking is an important concept developed for material science applications.[1,27–29] Topologically interlocking assemblies typically consist of identical congruent blocks that can be arranged in such a repeated way that the assembled structure is composed of rotated and translated versions of this prototype block and can be held together only by boundary constraints as mentioned earlier. Figure 1 provides an example of topological interlocking assemblies of regular polyhedra. In the example in Figure 1, there exists a plane that is a regular hexagonal grid, that is, it consists of regular planar hexagons with no gaps.[2] In each of these cases, if the bounding blocks are "fixed" (equivalently, if a peripheral force is applied to the bounding blocks), the internal blocks are kinematically constrained to hold their positions in space simply due to the geometric interfaces between the mutually neighboring blocks. In other words, in these assemblies, each block is kept in place by local kinematic constrains imposed through its shape and mutual arrangement of all the blocks.[1]

Interlocking can become stronger if there exist more than one plane that is composed by planar polygons with no gaps, along with local kinematic constraints. **Figure 5** provides an example of an assembly that consists of multiple stacked layers of planes that are composed by planar polygons with no gaps between them.[5]
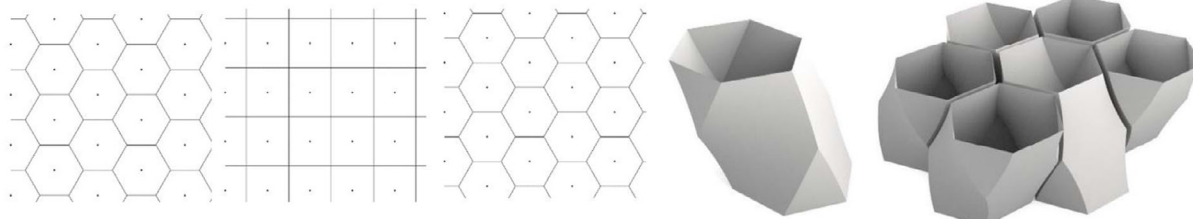
In such cases, block boundaries become ruled surfaces that can potentially improve local kinematic constrains.

Another important property of topological interlocking is that the layers do not have to be planar. For instance, the early historical examples of topological interlocking assemblies in ancient architecture have been spherical. Many ancient domes, such as Hagia Sofia, the world's largest interior space when it was built in 537 AD, were designed and constructed by such topological interlocking assemblies.[30–32] These buildings were erected using stones cut to be assembled into complex structures and held together by a global peripheral constraint.[1,27–29]

2.2. Topological Interlocking and Architecture

Medieval building masters have also employed topologically interlocking assemblies under different names. Early examples of similar assemblies, which are usually referred to as stereotomy, can be found in Villard de Honnecout's fylfot grillage assemblies, Leonardo da Vinci's spatial structures, Sebastiano Serlio's planar floors, and John Wallis's scholarly work.[33] In these constructions, a discrete load-bearing element supports two neighboring components and is mutually supported by two others to span distances longer than their length.[34–36] Other types of topologically interlocking assemblies are called nexorades,[37] referring to Asian forms of timber construction.[38]

Joseph Abeille obtained a patent in 1699 for a specific topologically interlocking assembly to construct flat structures, which are now known as Abeille vaults.[39] The congruent blocks of Abeille vaults are constructed by truncating two opposite edges of a tetrahedron. These blocks can be assembled in a two-directional pattern resembling a woven fabric to form self-supporting structures.[40,41] At about the same time, Sébastien Truchet also discovered and patented another topological interlocked assembly to construct flat surfaces.[31,42] One of the advantages of both Abeille's and Truchet's topologically interlocking assemblies is their ability to sustain loads and control the displacement of the tiles even for flat assemblies.[43–45] Both of these structural systems are capable of tolerating orthogonal and transverse forces.[46]

Topological interlocking assemblies lost their popularity[35,47] with the introduction of modern materials, such as Portland cement and reinforced concrete, during the 19th century.[48–50] They received renewed attention recently in architecture,[31,51] especially after the formalization of topological interlocking in material science.[1,2] However, most current research in *Architecture* has only focused on either analyzing existing

Figure 5. An example of topological interlocking assemblies that consist of cell-transitive 2-honeycombs stacked from the bottom to top.[5] These are obtained using curves in the form of $(x, y, z) = (f_x(t), f_y(t), t)$ as Voronoi sites and computing layer-by-layer Voronoi decomposition.[2] Therefore, each layer consists of congruent convex polygons and boundaries of the blocks are, therefore, ruled surfaces.[2]

**ADVANCED
SCIENCE NEWS**

www.advancedsciencenews.com

**ADVANCED
ENGINEERING
MATERIALS**

www.aem-journal.com

building blocks already proposed by Abeille and Truchet or creating curved structures from originally known blocks[31,42] with rare exceptions, cf. e.g.,.[52]

2.3. Geometric Principles for Topological Interlocking

Topological interlocking assemblies are also linked to the concept of 2-honeycombs, which are close packings of planar blocks so that there are no gaps between them.[53,54] If a 2-honeycomb consists of congruent (i.e., identical) planar tiles, it is called a cell-transitive (regular or isochoric) 2-honeycomb.[55] If any assembly of 3D blocks includes planar regions that correspond to a compact and connected subset of a 2-honeycomb, that planar region can potentially provide topological interlocking. If local kinematic constraints are satisfied, the blocks can hold together by applying a peripheral force on its boundary of closed curve.[2]

It is important to note that a deeper understanding of the mathematical formalization of 2-honeycombs is needed to design shapes that lead to topological interlocking assemblies based on Voronoi decomposition.[22] For instance, Figure 1 provides an example of a planar region that is a cell-transitive 2-honeycomb in some specific assembly of cubes. Moreover, all layers in the example in Figure 5 are cell-transitive 2-honeycombs that are stacked on top of each other.[5,6] However, note that this assembly is not completely interlocking, it is interlocking only in directions where the boundary of the shape contains a saddle point (specifically, a hyperbolic paraboloid in this case).

The standard mathematical model of an ideal crystal also involves a specific type of Delone sets, called symmetric (or crystal) sets,[56,57] which are invariant with respect to a crystallgraphic group.[22,56] The important property of symmetric Delone sets is that the Voronoi decomposition[58] of symmetric Delone sets in 3D can be used to obtain 3-honeycombs and space-filling congruent polyhedra.[22] The resulting space-filling congruent polyhedra are called plesiohedra.[18,59–61]

We observe that a 2D version of this approach can directly be applied to obtain cell-transitive 2-honeycombs and space-filling congruent flat blocks that could be called plesiogons.[18] To obtain layers of 2-honeycombs, the key component is the creation of layers of symmetric Delone sets that are invariant with respect to a wallpaper group. Our approach is inspired by the recent work by Subramanian et al. wherein they developed Delaunay lofts[5] by interpolating three (top, middle, and bottom) symmetric Delone sets to obtain all intermediate layers as symmetric Delone sets. This method generates a symmetric Delone set in every layer because the interpolation of Delone points corresponds to interpolations of underlying Bravais lattices.[26,62] Since these Delone sets comprise points, each layer of a Delaunay loft consists of only simple convex polygons. In other words, the boundaries of Delaunay lofts are either ruled or planar surfaces.

2.4. Knowledge Gaps and Our Work

A problem with interpolation is that the resulting assemblies of congruent blocks do not ensure topological interlocking. The occurrence of topological interlocking depends on the positions of the points in the top, middle, and bottom Delone sets. Therefore, there is no warranty an assembly will have the required local kinematic constraints. To overcome this issue, GATs have recently been developed.[6] The basic premise of GATs is the interpolation of multiple points to form trees. This flexibility allows one to proliferate a single polygon by generating a single polygon in one layer into multiple polygons in another layer, creating tree-like structures that can interlock better. Although this method is very powerful in obtaining strong interlocking, it requires creative interpolation approaches to obtain symmetric Delone sets. Comparing GATs, curve interpolation for Delaunay lofts is straightforward and guaranteed to work.

In this article, we used the Bravais lattice approach directly to obtain an infinite array of ruled surfaces. It is generated by two discrete Bravais translation operations. Each ruled surface is described by two trigonometric curves in z direction such that the intersection of the ruled surface with any $z = $ constant plane is either a point or a line. The only requirement for these two trigonometric curves is that they have to be continuous. Using appropriate Bravais translation vectors, we can always get a Delone set in every layer. When we use these ruled surfaces as Voronoi sites, the boundary between Voronoi regions is guaranteed to be corrugated thus providing strong topological interlocking. The advantage of this approach is its flexibility and simplicity for design.

3. Conceptual Framework

To present our approach, we first use an infinite array of a single curve as Voronoi sites. Such curves create spaghetti-like extruded structures with the same convex polygon-type cross sections along z direction, as shown in Figure 3d. We then extend these curves to ruled surfaces to obtain blocks that we dubbed Voronoi "Noodles" or VoroNoodles, for short.[63] In VoroNoodles, every layer can have a different cross section. Moreover, the shapes of cross sections can be nonconvex and boundary edges do not have to be straight. Therefore, *VoroNoodle* boundaries can be more complex than ruled surfaces.

3.1. Constant Cross-Section VoroNoodles

Consider a continuous curve $p : [0, 1] \rightarrow \Re^3$ defined as

$$\mathbf{p}(t) = (F_x(t), F_y(t), at) \tag{1}$$

where $t \in [0, 1]$ and a is any positive real number that is used to scale VoroNoodles along z direction. The functions $F_x : [0, 1] \rightarrow \Re$ and $F_y : [0, 1] \rightarrow \Re$ can be any functions as long as they are continuous. They do not need to be C^1 or C^2.

Now, assume that a Bravais lattice is defined by two linearly independent (but not necessarily mutually perpendicular) translation vectors $\mathbf{v}_0$ and $\mathbf{v}_1$ that can span the $x - y$ vector space given by the two orthonormal vectors $(1, 0, 0)$ and $(0, 1, 0)$. We use this Bravais lattice to produce an infinite array of curves by adding the vector $n_0 \vec{v}_0 + n_1 \vec{v}_1$ to the curve as

**ADVANCED
SCIENCE NEWS**

www.advancedsciencenews.com

**ADVANCED
ENGINEERING
MATERIALS**

www.aem-journal.com

$$\mathbf{p}(t) + n_0\vec{v}_0 + n_1\vec{v}_1 \tag{2}$$

where n_0 and n_1 are any integers that span the lattice. Regardless of how we choose the functions F_x and F_y and the Bravais vectors v_0 and v_1

$$\mathbf{p}(0) + n_0\vec{v}_0 + n_1\vec{v}_1 \tag{3}$$

has to be a symmetric Delone set that consists of points only. Its symmetry is uniquely defined by the vectors $\mathbf{v}_0$ and $\mathbf{v}_1$, as shown in **Figure 6**. For any given t, we obtain only a translated version of the same symmetric Delone set, such as in Figure 6c. Therefore, this formulation can be considered an extrusion of symmetric Delone set along the curve $\mathbf{p}(t)$. The type of extrusion is uniquely defined by the choice of the functions F_x and F_y.

Now, let $0 \leq s_0 \leq 1$, and $0 \leq s_1 \leq 1$ be real numbers; then, following set of line segments with beginning and ending points

$$\begin{aligned} p_0(t) &= \mathbf{p}(t) + n_0\vec{v}_0 + n_1\vec{v}_1 \quad \text{and} \\ p_1(t) &= \mathbf{p}(t) + (n_0 + t_0)\vec{v}_0 + (n_1 + t_1)\vec{v}_1 \end{aligned} \tag{4}$$

also forms a Delone set of lines. If we apply a 2D Voronoi tessellation in each of these Delone sets in each layer, we obtain the same 2-honeycomb in each layer. As a result, this will give us an extrusion of a 2-honeycomb defined by the Bravais lattice along with the curve $\mathbf{p}(t)$ or $\mathbf{p}(z)$. In other words, these congruent blocks that comprise the same convex and congruent polygons that are stacked on top of each other. These shapes will really look like long and skinny spaghetti if $|\vec{v}_0| \ll 1$ and $|\vec{v}_1| \ll 1$, as shown in Figure 3. The shape of convex and congruent polygons depends only on relative orientations and lengths of Bravais vectors $\vec{v}_0$ and $\vec{v}_1$. The shape can be a square, a rectangle, a regular hexagon, or a general hexagon.

3.2. Variable Cross-Section VoroNoodles

Let us introduce a vector curve defined on $[0,1] \rightarrow [0,1)^2$ as

$$\vec{v}(t) = G_x(t)\vec{v}_0 + G_y(t)\vec{v}_1 \tag{5}$$

where $t \in [0,1]$ and the functions $G_x:[0,1] \rightarrow [0,1)$ and $G_y:[0,1] \rightarrow [0,1)$ are continuous. Now, consider the ruled surface that is defined by the following equation.

$$\mathbf{p}(t,u) = \mathbf{p}(t)(1-u) + (\mathbf{p}(t) + \vec{v}(t))u \tag{6}$$

This ruled surface consists of lines in every $z = $ constant layer. Further consider an infinite array of these ruled surfaces as a Bravais lattice by adding the vector $n_0\vec{v}_0 + n_1\vec{v}_1$ to the surface as

$$\mathbf{p}(t,u) + n_0\vec{v}_0 + n_1\vec{v}_1 \tag{7}$$

where the coefficients n_0 and n_1 are any integers to span the lattice. In these cases, regardless of how we choose the vector function $\vec{v}(t)$, the infinite array of ruled surfaces never intersect with each other since we chose the two components of the vector function to be smaller than $|\vec{v}_0|$ and $|\vec{v}_1|$ respectively. Therefore, the line segment will always stay within the parallelogram defined by the Bravais vectors $\vec{v}_0$ and $\vec{v}_1$ (See Figure 6).

This property is useful since we can formally ensure each layer to be a symmetric Delone set.[25,57] This is based on Dolbilin's result[56,57] that demonstrates the following; if n-number of symmetric Delone sets represent the same crystallographic (in 2D wallpaper) group, their union also represents the same wallpaper group with a crystallographic orbit of n-number points. Using this result, it is possible to be arbitrarily close to any given higher-dimensional shape, such as a planar curve, which can result from 2D crystals. Now, assume that we replace points in a symmetric Delone set with lines. Their Voronoi decomposition permits the creation of cell-transitive 2-honeycombs with congruent planar plesiogon shapes that can have curved edges.

This is not the only method to obtain 2D Delone sets of lines. For instance, we can start with any two curves $\mathbf{p}_0(t)$ and $\mathbf{p}_1(t)$, and we can obtain any ruled surface as

$$\mathbf{p}(t,u) = \mathbf{p}_0(t)(1-u) + \mathbf{p}_1(t)u \tag{8}$$

For this ruled surface, we can always construct two Bravais vectors using two given direction $\vec{n}_0$, and $\vec{n}_1$ as $\vec{v}_0 = a_0\vec{n}_0$, and $\vec{v}_1 = a_1\vec{n}_1$ by choosing a_0 and a_1 large enough to avoid intersection regardless of how initial curves are chosen. Note that the choice of $\vec{n}_0$, and $\vec{n}_1$ and a_0 and a_1 is not unique for any given set of two curves that define a ruled surface.

In conclusion, this particular approach provides a large design space to construct topologically interlocking assemblies by generating a different symmetric Delone set in every layer for any set of curves and Bravais vectors. If the lines are not identical for all $z = $ constant planes, the Voronoi partition of each layer produces a different congruent planar shape, as shown in **Figure 7**, by providing additional local constraints.
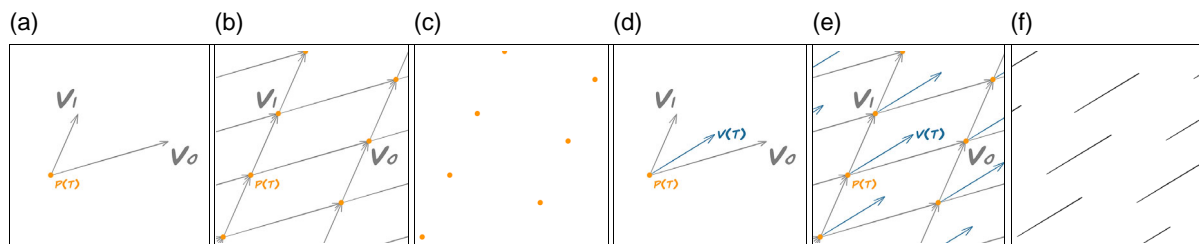

Figure 6. Bravais vectors define a Delone set and the line in each layer will stay inside of the parallelogram defined by the Bravais vectors $\vec{v}_0$ and $\vec{v}_1$. a) Initial point and Bruvais vector in Layer t; b) Bruvais translation of the point in layer t; c) Delone set of points in layer t; d) Initial line in layer t; e) Bravais translation of lines in layer t; f) Delome set of lines in layer t.
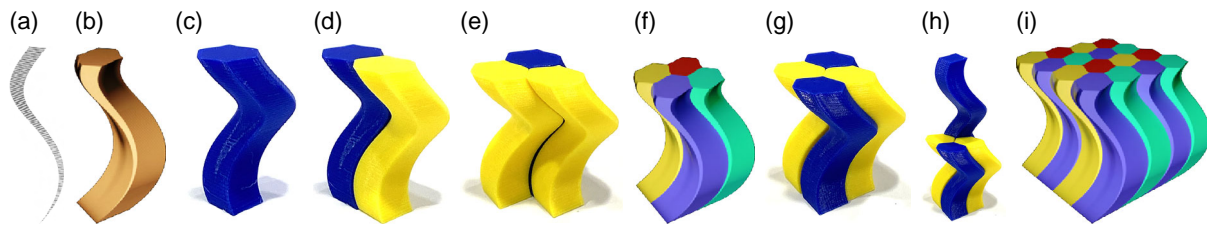
Figure 7. An example of VoroNoodles with a different 2-honeycomb in each layer. This is obtained using a ruled surface as a Voronoi site, created by scaling a line. Each layer is translated using the function $\mathbf{p}(t)$ in the form of $x = \cos(2\pi t)$, $y = \sin(2\pi t)$, and $z = t$ to create a helix. For $\vec{v}(t)$, we scaled and rotated a 2D vector. a) Ruled surface; b) Single VoroNoodle; c) Printed single VoroNoodle; d) Assemble of two printed VoroNoodles; e) Assemble of three printed VoroNoodles; f) Rendered assemble of four VoroNoodles; g) Assemble of four printed VoroNoodles; h) Five VoroNoodles; i) Ruled Surface that is used as Voronoi site. Reproduced under terms of the CC BY-NC-ND 4.0, Copyright 2022, published by Cassie Mullins, Matthew Ebert, Ergun Akleman, and Vinayak Krishnamurthy.[63]

4. Tile Generation Methodology

We present a construction methodology using an extruded 3×3 Bravais lattice that is given by nine parallelograms given by $\vec{v}_0$ and $\vec{v}_1$. **Figure 8** demonstrates the steps of the process devised to obtain one cross section of a *VoroNoodle* for a given layer. While we implemented this process in Houdini and Python software, this algorithm can be used in many other programs and coding languages. The process consists of the following steps.

1) Sample

$$\mathbf{p}(t, u) = \mathbf{p}(t)(1 - u) + (\mathbf{p}(t) + \vec{v}(t))u \tag{9}$$

in the parameters t and u in $[0, 1]^2$ with $(N + 1) \times (M + 1)$ equal samples as $t_i = i/N$ where $i = 0, 1, \ldots, N$ and $u_j = j/M$ where $j = 0, 1, \ldots, M$.

2) Create a 3×3 Bravais lattice $\vec{v}_0 \times \vec{v}_1$ in each layer using $\mathbf{p}(t_i)$ as its center point as shown in Figure 8b. These are parallelograms that can actually correspond to bivectors of geometric algebra $9\vec{v}_0 \times \vec{v}_1$. This operation creates a crystal with $9 \times (N + 1) \times (M + 1)$ unit cells.

3) Classify the nine set of points into two groups using one label for the points that belong to the original ruled surface $\mathbf{p}(t, u)$ and another label for all other points. A cross section of lines is shown in Figure 8c.

4) Decompose the 3×3 parallelogram region using points as Voronoi sites and take the union of the Voronoi regions that share the same label. The process creates two volumetric regions. The Voronoi region that comes from the ruled surface $\mathbf{p}(t, u)$ is the VoroNoodle. The union of the rest provides a shape that can be used as a mold for VoroNoodle. A cross section is shown in Figure 8e. Note that even the planar cross-section region is not

necessarily convex or polygonal. Boundaries most likely are parabolic curves in these cross sections, as shown in Figure 8e.

5. Finite-Element Modeling

In order to perform systematic testing of the structures, we limit our focus to constant cross-section noodle geometries, that is, tiles that are identical at every layer. Furthermore, as the goal of this work is to perform initial testing of the structures, we only used a square cross-sectional layer. It is possible in future work to use different 2D tesselation patterns or to extend the work to VoroNoodles where layers change throughout the height of the blocks. We controlled the resolution of the shape to be identical, meaning that the square at each layer for every test is the same size. Additionally, the height of the block as well as the radius and pitch of the helix were varied to create several different structures.

5.1. Interfacing Criteria: Stepped Versus Smooth

While stacking of 2D Voronoi layers simplifies the creation process, a number of problems arise when using the mesh for FEA. For a small number of stacked layers, stress concentrations are formed because of the steps (**Figure 9**a). In order to avoid this, a large number of steps can be taken to approximate a smooth mesh so that there are no stress concentrations. This is often the case for the blocks shown in this work. The problem with this approach is that the resulting mesh requires a very high resolution and can increase computational time manyfold with a high number of layers.
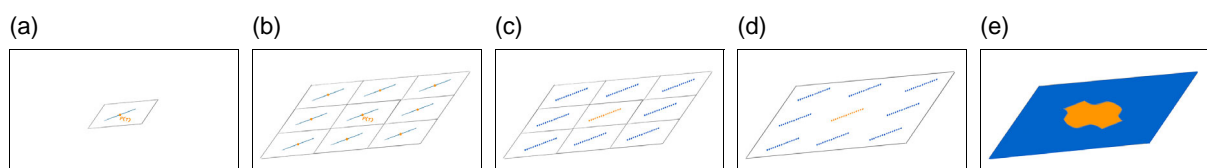

Figure 8. The process of construction of VoroNoodle shapes shown in a planar cross section. (Note labeling by color). a) The parallelogram and the line in layer t; b) 3×3 parallelograms in layer t.; c) Labeling the lines to partition them into two groups; d) Sampling the lines. The sampled points inherit the original labels. e) Voronoi decomposition by using two types of Voronoi sites. Reproduced under terms of the CC BY-NC-ND 4.0, Copyright 2022, published by Cassie Mullins, Matthew Ebert, Ergun Akleman, and Vinayak Krishnamurthy.[63]
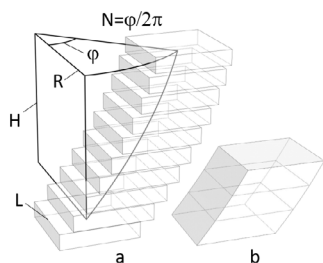
Figure 9. Schematics of the VoroNoodle geometry for FEM simulations: a) stepped and b) smoothed geometry.

In order to keep the benefit of a low-resolution mesh while also ensuring no stress concentrations, we employ a method that smooths a rough stepped mesh. When designing VoroNoodles with point sites, each layer is identical to the layers above and below; using this fact, instead of thickening a given layer, the mesh is triangulated by connecting points from adjacent layers. This results in an approximately smooth block that does not develop any stress concentrations between layers (Figure 9b). Another perspective is that since every layer is an identical polygon, the resulting approximately smooth geometry is just a sweep of the polygon. This process allows for a lower-resolution mesh to be used while maintaining the benefit of a smooth mesh.

5.2. Computational Model

The study of the mechanical properties of interlocked Voronoi noodles was carried out using finite-element modeling in the dynamic explicit mode using the ABAQUS software package. As a material model, a homogeneous, isotropic linear–elastic body with the Young's modulus of $E =$ GPa and Poisson's ratio of $\nu = 0.3$ was chosen. The contact interaction between the blocks was set considering the normal component (hard contact) and the tangential component in the form of the Coulomb friction law with a friction coefficient of 0.3. The calculation involved nine blocks. For all blocks except the central one, the boundary conditions in the form of rigid embedment (displacements equal to zero) were applied along the outer perimeter. The geometric parameters varied in these finite element method (FEM) simulations are shown in Figure 9. As follows from the general description of the geometric features of a block, there are many more variable geometry parameters. Based on the experience with preliminary modeling of Voronoi noodles, four main parameters were identified, and their influence was studied in this work. The dimensionless parameters H/L and R/L are the characteristics of the noodle length and the distance of a cross section from the center of the helix. The cross section of the noodles, a square with side L, and the pitch of the helix were constant along a noodle. To characterize the angle of rotation ϕ, the number of revolutions N was used (which is generally not an integer). Also, one of the important factors is the method of connecting the "slices" of a noodle. The stepped method (Figure 9a) has many advantages, as mentioned earlier, since it allows one to connect the "slices" along a generating curve of any geometry, which greatly simplifies the design. When the step size tends

to 0, the geometry of the noodle is transformed to the smoothed type (Figure 9b). The effect of this factor will be discussed in more detail below, in the discussion section. Here we only note that the smoothed geometry is preferable from the point of view of FEM. Accordingly, most of the modeling was done for these types of noodles. A list of the parameters used in computational experiments is presented in **Table 1**.

6. Results

Figure 10 shows the distribution of stresses in the assemblies at the initial stage of displacement of the intender loading applied to the central block. For all the options considered, the stress distribution is significantly nonuniform, which is associated with the asymmetry of the block. The blocks 2 and 4 exhibit the highest contact stresses. The stresses are distinctly lower in the assemblies shown in the upper row (Figure 10a,c,e,g,i), which unambiguously correlates with the shorter noodle length. The greater length of the noodle (Figure 10b,d,f,h,j), as well as a greater rotation angle, lead to the rise of the resistance to the removal of the central block for the block geometries 8 and 6. Qualitatively, the distribution of stresses in the assembly for geometries with stepped architecture (Figure 10i,j) does not differ from the smooth type, but quantitatively, the stresses in the former case turned out to be almost an order of magnitude higher.

Figure 11 shows the distribution of stresses in the central block. The stress state of the inner blocks correlates well with the stresses acting on the outer blocks, as depicted in Figure 10. An increase of the length of the noodles leads to an increase in stress. The stress distributions in the blocks seen in the bottom row show that nearly the entire block is deformed, while the blocks of the top row have a significant part remaining in the undeformed state. The variation of the radius of the helix affects the stress distributions to a much lesser extent, but the trend of increasing stress with increasing radius can be observed still. A significant difference between smoothed and stepped blocks is quite remarkable. In the latter, the stresses are much higher and localized within the steps, rather than extending over the whole block.

The simulation results in the form of the force versus indenter displacement dependence are presented in **Figure 12**. The

Table 1. Summary of the FEM simulations conducted.

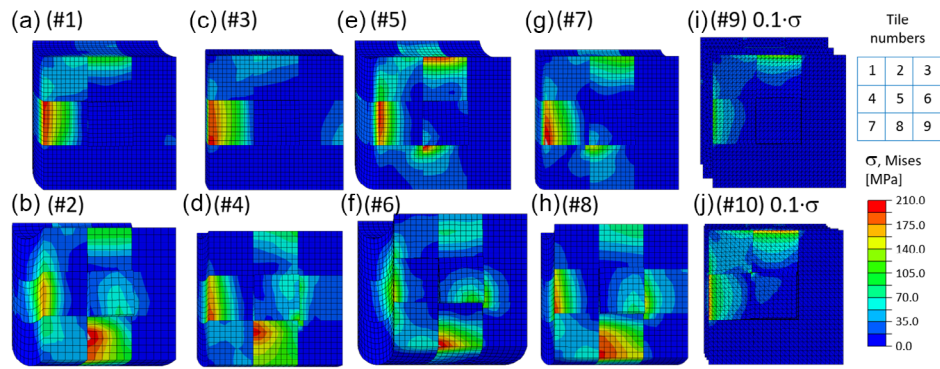| Test number	H/L	R/L	$N\,[\phi,°]$	Noodle geometry
1	0.6	0.5	0.2 [72]	Smoothed
2	1.2	0.5	0.4 [114]	Smoothed
3	0.6	0.25	0.2 [72]	Smoothed
4	1.2	0.25	0.4 [144]	Smoothed
5	0.6	0.5	0.3 [108]	Smoothed
6	1.2	0.5	0.5 [180]	Smoothed
7	0.6	0.25	0.3 [108]	Smoothed
8	1.2	0.25	0.5 [180]	Smoothed
9	0.6	0.5	0.2 [72]	Stepped
10	1.2	0.25	0.4 [144]	Stepped

2300831 (8 of 12)

Figure 10. Distribution of the von Mises equivalent stresses in the assembly. Extraction of the central block is carried out in the viewing direction. (The label of each part corresponds to the varients listed in Table 1).
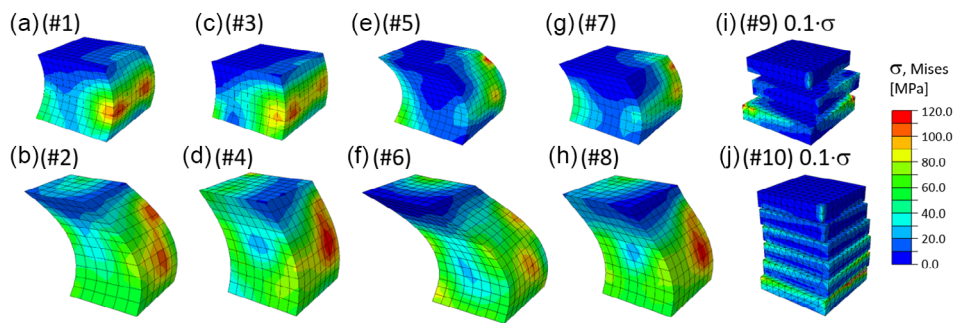

Figure 11. Distribution of the von Mises equivalent stresses in the central block. (The label of each part corresponds to the varients listed in Table 1).
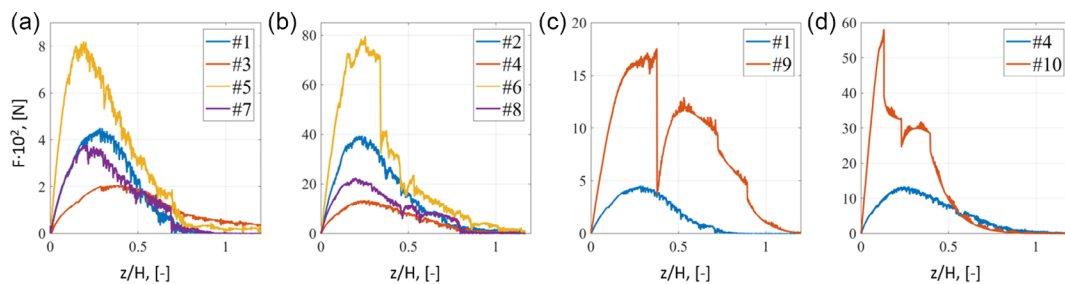

Figure 12. Force–displacement diagrams for different kinds of blocks: a) short smoothed, b) long smoothed, c) short smoothed versus stepped, d) long smoothed versus stepped. (The numbers correspond to the variants listed in Table 1).

characteristic skewed parabolic shape of the curves is typical for interlocking materials; see refs..[52,64,65] In all cases, the load increases rapidly and drops off after reaching a peak. The rate of decrease is smaller than the rate of growth. An increase in the length of the noodle, the radius of the helix, and the degree of rotation lead to an increase in the force required to extract the block from the assembly. Although increasing the length and increasing the degree of twist raises the engagement force, these parameters are highly correlated, so it is difficult to assess their separate influence at this stage. The type of interlocking also has a very strong effect on the engagement force. As shown in Figure 12c,d, with the same other noodle parameters, the stepped surface gives rise to a force that is a multiple of the force associated with a smooth surface.

7. Discussion

From a geometric modeling perspective, it it natural to imagine that the type of tiles presented in this work could be generated using 3D (i.e., volumetric) Voronoi tessellation for a set of helical sites wherein each helix curve is one site rather than a layered collection of points. Here, our choice of using layer-by-layer strategy in contrast to 3D Voronoi decomposition played a critical role in terms of 1) controlling the level of corrugation, 2) the genus (i.e., the number of holes) of generated tiles, and 3) the ability to generate, assemble and disassemble tiles (see **Figure 13** for a comparison between 3D and layerwise or 2.5D strategy).

An analysis of the influence of the geometric parameters of the VoroNoodle on the mechanical behavior of the assembly shows
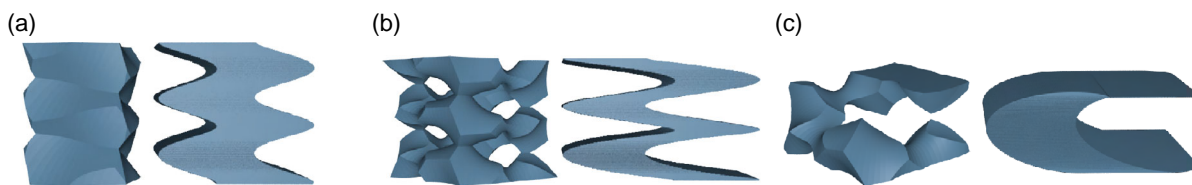
Figure 13. Comparison of 3D versus 2.5D (i.e., layer-by-layer) Voronoi decomposition[5] using the same datasets. Note that 3D Voronoi can even produce high-genus tiles that may not necessarily be assembled. 2.5D provides strong corrugations and guarantees to create genus-0 surfaces. a) 3D Voronoi at the left does not provide strong corrugarion; b) 3D Voronoi at the left is not genus-0; c) 3D Voronoi at the left cannot be disassembled. Reproduced under terms of the CC BY-NC-ND 4.0, Copyright 2022, published by Cassie Mullins, Matthew Ebert, Ergun Akleman, and Vinayak Krishnamurthy.[63]

their very strong effect. The proposed block architecture allows, by varying the geometry in a small window of parameters (see. Table 1), to change the engagement force by almost an order of magnitude. In this study, we deliberately narrowed the ranges of variation of geometric parameters. This was because this architecture allows an assembly to go into a state of complete jamming very quickly. For example, in case 1 for $N = 1$, all other parameters being the same, extracting the loaded central block is no longer possible. This distinctive feature makes the architecture of VoroNoodle assemblies attractive due to the extremely high sensitivity of mechanical properties to the design parameters. However, our statement about the possibility of complete blocking holds true only when considering linear elasticity. The engagement force increases as the contact surface grows. As long as the element has a small contact surface, it can be pushed (or pulled) out of the assembly, while its behavior remains consistent with the linear elastic model. However, with an increase in the contact surface, the ejection forces and contact stresses increase and the calculation becomes less meaningful when the stresses exceed those corresponding to the elastic regime and nonlinearity or plasticity set in. Another feature of

this architecture is the entanglement of the interlocked blocks. While for many other topological or geometrical interlocked structures, it is possible to push or pull out a locally loaded block from the assembly; to achieve that for VoroNoodle, the indenter would have to move along the corresponding helix. There are known examples of helical architectures that show a remarkably high load-bearing capacity of the assembly due to high resistance to crack propagation.[66,67] This may also be the case for the VoroNoodle architecture considered in the article. The concomitant increase in fracture toughness is an aspect that needs to be explored further in future work.

The method is not limited to flat assemblies only. It is possible to construct more complicated shapes by bijective transformations, as shown in **Figure 14** and **15**. Note that the congruence property of the corrugated blocks can be preserved for some bijective mapping such as scale, shear, or cylindrical transformations (see Figure 14 for a cylindrical assembly of congruent corrugated blocks). However, for many bijective transformations, it is not preserved. The resulting corrugated block appears similar but not exactly the same (see Figure 15 for a dome assembled from noncongruent corrugated blocks).
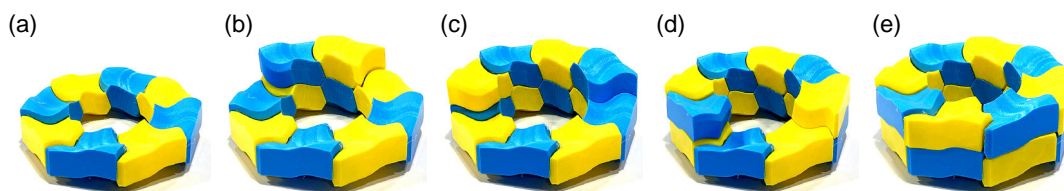

Figure 14. An example of congruent VoroNoodles on a cylindrical domain. a) Cylindrical assembly of eight printed VoroNoodles; b) Cylindrical assemble of ten printed Voronoodles; c) Cylindrical assembly of 12 printed VoroNoodles; d) Cylindrical assembly of 14 printed Voronoodles; e) Cylindrical assembly of 16 printed VoroNoodles. Reproduced under terms of the CC BY-NC-ND 4.0, Copyright 2022, published by Cassie Mullins, Matthew Ebert, Ergun Akleman, and Vinayak Krishnamurthy.[63]
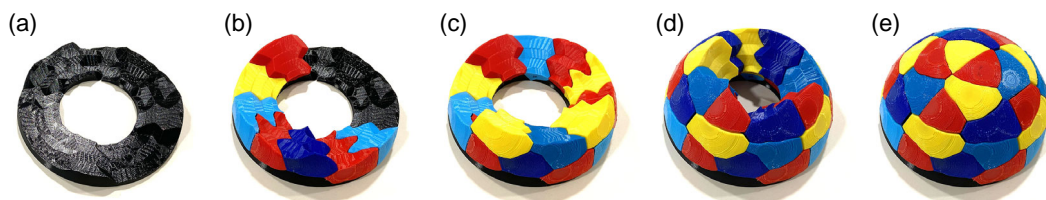

Figure 15. An example of noncongruent VoroNoodles on a spherical domain. Reproduced under terms of the CC BY-NC-ND 4.0 a) Base for Dome Construction; b) Dome Construction with seven printed VoroNoodles; c) Dome Construction with 15 printed VoroNoodles; d) Dome Construction with 26 printed VoroNoodles; e) Dome construction with 34 printed VoroNoodles. Copyright 2022, published by Cassie Mullins, Matthew Ebert, Ergun Akleman, and Vinayak Krishnamurthy.[63]
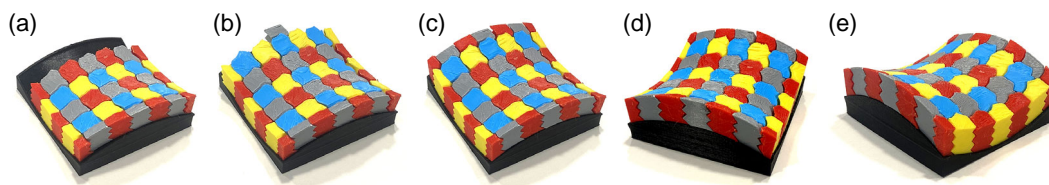
Figure 16. Another example of noncongruent VoroNoodles on a hyperbolic paraboloid saddle domain. Corrugated boundaries between the blocks are clearly visible. d) Saddle shape example with 35 blocks; b) saddle shape example with 43 blocks; c) saddle shape example with 49 blocks; d) Another view of the saddle shape; e) A further view of saddle shape with 49 blocks. Reproduced under terms of the CC BY-NC-ND 4.0, Copyright 2022, published by Cassie Mullins, Matthew Ebert, Ergun Akleman, and Vinayak Krishnamurthy.[63]

8. Conclusion

In this article, we presented a new class of segmented structures that extends the repertoire of topological interlocking-based design. At the core of it is a combination of Voronoi tessellation of a plane with a particular recipe for proliferating it in the direction normal to the plane along helical ruled surfaces. The resulting volumetric bodies—the building blocks of a 3D assembly we dubbed VoroNoodles—are space-filling shapes. A recipe for VoroNoodle design based on the concept of Delone sets has been outlined. Examples of topologically interlocked planar, cylindrical, spherical, and saddle-point assemblies constructed from such building blocks have been given in **Figure 16**.

The spiral shape and full interlockability of the blocks promise interesting mechanical properties. First finite-element calculations presented in the article have demonstrated that VoroNoodle-based assemblies exhibit mechanical response in terms of the force–displacement profile–a skewed inverse parabola that is qualitatively similar to that known for the polyhedra-based topological interlocking structures.

The FEM simulations conducted for an idealized isotropic linear–elastic model material have revealed a strong effect of a secondary step relief on the surface of a VoroNoodle on the force level under concentrated load applied to the middle block. What is remarkable is the sensitivity of this response to the geometric parameters: by varying the radius and pitch of the helix within a narrow range, radically different behavior has been demonstrated.

Even though this work demonstrates the geometric modeling of variable cross-section noodles, the parameter space for enumerating different designs for these varieties is exceptionally large. Therefore, our study was focused on evaluating the effect of corrugation using constant cross-sectional noodles which are easier to parametrize. Using point sites allowed us to shed light on the mechanical properties of corrugation-based interlocking. The variable cross-section cases are important for further development of VoroNoodle design, which will be the focus of our future work. We recognize that with the present study, we just scratched the surface of a huge hidden repository of topological interlocking structures yet to be uncovered. This should be motivation for further investigations in this area.

Acknowledgements

Conflict of Interest

The authors declare no conflict of interest.

Data Availability Statement

The data that support the findings of this study are available from the corresponding author upon reasonable request.

Keywords

[1] A. Dyskin, Y. Estrin, A. Kanel-Belov, E. Pasternak, *Scr. Mater.* **2001**, *44*, 2689.

[2] Y. Estrin, V. R. Krishnamurthy, E. Akleman, *J. Mater. Res. Technol.* **2021**, *15*, 1165.

[3] Y. Estrin, Y. Bréchet, J. Dunlop, P. Fratzl, *Architectured Materials in Nature and Engineering*, Springer Nature Switzerland AG, Cham, Switzerland **2019**.

[4] Y. Estrin, Y. Beygelzimer, R. Kulagin, P. Gumbsch, P. Fratzl, Y. Zhu, H. Hahn, *Mater. Res. Lett.* **2021**, *9*, 399.

[5] S. G. Subramanian, M. Eng, V. R. Krishnamurthy, E. Akleman, *Comput. Graph.* **2019**, *82*, 73.

[6] E. Akleman, V. R. Krishnamurthy, C.-A. Fu, S. G. Subramanian, M. Ebert, M. Eng, C. Starrett, H. Panchal, *Comput. Graph.* **2020**, *89*, 156.

[7] F. Barthelat, *Int. Mater. Rev.* **2015**, *60*, 413.

[8] U. G. Wegst, H. Bai, E. Saiz, A. P. Tomsia, R. O. Ritchie, *Nat. Mater.* **2015**, *14*, 23.

[9] P. Fratzl, R. Weinkamer, *Prog. Mater. Sci.* **2007**, *52*, 1263.

[10] H. Chen, Y. Liu, C. Wang, A. Zhang, B. Chen, Q. Han, J. Wang, *Comput. Biol. Med.* **2021**, *130*, 104241.

[11] W. Clegg, K. Kendall, N. M. Alford, T. Button, J. Birchall, *Nature* **1990**, *347*, 455.

[12] J. Baucom, J. Thomas, W. Pogue III, M. S. Qidwai, *J. Compos. Mater.* **2010**, *44*, 3115.

[13] D. Li, Y. Li, W. Yu, B. Wang, P. Lu, S. Shen, *Compos. Struct.* **2020**, *243*, 112179.

[14] X. Tang, X. Yan, *Composites, Part A* **2017**, *101*, 360.

[15] L. Tadrist, M. Miscevic, O. Rahli, F. Topin, *Exp. Therm. Fluid Sci.* **2004**, *28*, 193.

[16] M. Ansar, W. Xinwei, Z. Chouwei, *Compos. Struct.* **2011**, *93*, 1947.

[17] B. Behera, B. Dash, *Mater. Des.* **2015**, *67*, 261.

[18] B. Grünbaum, G. C. Shephard, *Bull. Am. Math. Soc.* **1980**, *3*, 951.

[19] V. R. Krishnamurthy, E. Akleman, S. G. Subramanian, M. Ebert, J. Cui, C.-a. Fu, C. Starrett, *IEEE Trans. Vis. Comput. Graph* **2021**, *27*, 3391.

[20] A. N. Karuriya, F. Barthelat, *Proc. Natl. Acad. Sci.* **2023**, *120*, e2215508120.

[21] B. N. Delone, *The St. Petersburg School of Number Theory*, Vol. *26*, American Mathematical Society, Providence, RI **2005**.

[22] B. N. Delaunay, N. N. Sandakova, *Tr. Mat. Inst. im. VA Steklova* **1961**, *64*, 28.

[23] M. W. Schmitt, *Ph.D. Thesis*, Freien Universität Berlin, **2016**.

[24] B. N. Delone, N. P. Dolbilin, S. Ryškov, M. Štogrin, *Math. USSR-Izv.* **1970**, *4*, 293.

[25] B. N. Delone, N. P. Dolbilin, M. I. Shtogrin, R. V. Galiulin, *Dokl. Akad. Nauk SSSR* **1976**, *227*, 19.

[26] A. Bravais, *J. Ecole Polytechn.* **1850**, *1*, 1.

[27] A. V. Dyskin, Y. Estrin, A. J. Kanel-Belov, E. Pasternak, *Philos. Mag. Lett.* **2003**, *83*, 197.

[28] A. Dyskin, Y. Estrin, E. Pasternak, in *Architectured Materials in Nature and Engineering* Springer, New York **2019**, pp. 23–49.

[29] Y. Estrin, A. V. Dyskin, E. Pasternak, *Mater. Sci. Eng. C* **2011**, *31*, 1189.

[30] R. Evans, *The Projective Cast: Architecture and its Three Geometries*, MIT Press, Cambridge, MA **1995**.

[31] G. Fallacara, in *Proc. of the Third Int. Congress on Construction History*, Short Run Press **2009**, p. 553.

[32] S. Fernando, R. Saunders, S. Weir, *Future Archit. Res.* **2015**, *82*, 83.

[33] D. Yeomans, *Arch. Res. Q.* **1997**, *2*, 74.

[34] A. Pugnale, D. Parigi, P. H. Kirkegaard, M. S. Sassone, in *The 35th Annual Symp. of the IABSE 2011, the 52nd Annual Symp. of the IASS 2011 and Incorporating the 6th Int. Conf. on Space Structures*, International Association for Bridge and Structural Engineering (IABSE)/IASS **2011**, pp. 414–421.

[35] M. Brocato, L. Mondardini, *Int. J. Solids Struct.* **2012**, *49*, 1786.

[36] M. Weizmann, O. Amir, Y. J. Grobman, *Autom. Constr.* **2016**, *72* 18.

[37] O. Baverel, H. Nooshin, Y. Kuroiwa, G. Parke, *Int. J. Space Struct.* **2000**, *15*, 155.

[38] M. Brocato, L. Mondardini, *Int. J. Solids Struct.* **2015**, *54*, 50.

[39] J.-G. Gallon, *Machines Et Inventions Approuvées Par L'Academie Royale Des Sciences Depuis Son Établissement Jusqu'à Présent; Avec Leur Description*, Vol. *7*, Chez Gabriel Martin, Jean-Baptiste Coignard, Hippolyte-Louis Guerin, Paris **1777**.

[40] A. Borhani, N. Kalantar, in *ShoCK!-Sharing Computational Knowledge!: Proc. of the 35th eCAADe Conf.*, Vol. *1*, eCAADe **2017**, pp. 639–648.

[41] I. M. Vella, T. Kotnik, *Sharing of Computable Knowledge!*, eCAADe **2017**, pp. 251–259.

[42] A. Frézier, *La théorie et la pratique de la coupe des pierres et des bois pour la construction des voûtes et autres parties des baâtiments civils et militaires*, Jacques Laget LAME, Nogent-le-Roy **1737**.

[43] I. M. Vella, T. Kotnik, *Geometric Versatility of Abeille Vault*, eCAADe **2016**, https://papers.cumincad.org/data/works/att/eCAADe_2016_volume2_screen_lowres_SCOPUS.pdf#page=391.

[44] O. Tessmann, M. Becker, in *18th Int. Conf. on Computer-Aided Architectural Design Research in Asia: Open Systems, CAADRIA 2013; Singapore; Singapore; 15 May 2013 through 18 May 2013*, The Association for Computer-Aided Architectural Design Research in Asia (CAADRIA), Hong Kong, and Center for Advanced Studies in Architecture (CASA), Department of Architecture, School of Design and Environment, National University of Singapore, Singapore, **2013**, pp. 469–478.

[45] F. Fleury, in *Proc. of the Third Int. Congress on Construction History*, NEUNPLUS1 **2009**, pp. 101–109.

[46] M. Brocato, W. Deleporte, L. Mondardini, J.-E. Tanguy, *Int. J. Space Struct.* **2014**, *29*, 97.

[47] M. Brocato, L. Mondardini, *Advances in Architectural Geometry 2010*, **2010**, pp. 149–162.

[48] E. R. Daz, in *Actas Del Segundo Congreso Nacional De Historia De La Construcción, A Coruna*, Reverte **1998**, pp. 22–24.

[49] R. Courland, *Concrete Planet: The Strange and Fascinating Story of The World's Most Common Man-Made Material*, Prometheus Books, Amherst, NY **2011**.

[50] P. Jahren, T. Sui, *History of Concrete: A Very Old and Modern Material*, World Scientific, Singapore **2017**.

[51] G. Fallacara, in *Proc. of the Second Int. Congress on Construction History*, Vol. *1*, Short Run Press **2006**, pp. 1075–1092.

[52] M. Mirkhalaf, T. Zhou, F. Barthelat, *Proc. Natl. Acad. Sci.* **2018**, *115*, 9128.

[53] H. S. M. Coxeter, in *Conf. Board on the Mathematical Sciences: Regional Conf. Series in Mathematics*, American Mathematical Society, Providence, RI **1970**.

[54] H. S. M. Coxeter, in *Proc. of the Int. Congress of Mathematicians*, Vol. *3*, Citeseer, **1954**, pp. 155–169.

[55] H. S. M. Coxeter, *Regular Polytopes*, Courier Corporation, **1973**.

[56] N. Dolbilin, in *Geometry and Symmetry Conf*, Springer, New York **2015**, pp. 109–125.

[57] N. Dolbilin, A. Garber, U. Leopold, E. Schulte, M. Senechal, *Discrete Comput. Geom.* **2021**, *66*, 996.

[58] G. Voronoi, *J. Reine Angew. Math.* **1908**, *1908*, 198.

[59] R. M. Erdahl, *Eur. J. Comb.* **1999**, *20*, 527.

[60] A. Pugh, *Polyhedra (Close-Packing Polyhedra)*, University of California Press, downtown Oakland, CA **2020**.

[61] A. H. Schoen, On the graph (10,3)-a, **2008**, https://www.ams.org/journals/notices/200806/200806-full-issue.pdf?cat=fullissue&trk=fullissue200806.

[62] A. Mois, U. Müller, H. Wondratschek, *Historical Introduction: International Tables for Crystallography*, Springer **2006**.

[63] C. Mullins, M. Ebert, E. Akleman, V. Krishnamurthy, in *SIGGRAPH Asia 2022 Technical Communications*, Association for Computing Machinery **2022**, pp. 1–4.

[64] T. Siegmund, F. Barthelat, R. Cipra, E. Habtour, J. Riddick, *Appl. Mech. Rev.* **2016**, *68*, 4.

[65] L. Djumas, G. P. Simon, Y. Estrin, A. Molotnikov, *Sci. Rep.* **2017**, *7*, 11844.

[66] Y. Gao, B. Li, J. Wang, X.-Q. Feng, *J. Mech. Phys. Solids* **2021**, *146*, 104206.

[67] Y. Politi, L. Bertinetti, P. Fratzl, F. G. Barth, *Philos. Trans. R. Soc. A* **2021**, *379*, 20200332.